Published in final edited form as:
J Immunol. 2008 June 1; 180(11): 7497–7505.

SHIP-1 Increases Early Oxidative Burst and Regulates Phagosome Maturation in Macrophages[1]:

SHIP-1 regulates macrophage oxidase activity

Lynn A. Kamen[*,†], **Jonathan Levinsohn**[*], **Amy Cadwallader**[*], **Susheela Tridandapani**[††], and **Joel A. Swanson**[*,†]

[*] Department of Microbiology and Immunology, University of Michigan Medical School, Ann Arbor, MI 48109-0620

[†] Program in Immunology, University of Michigan Medical School, Ann Arbor, MI 48109-0620

[††] Department of Internal Medicine, Ohio State University, Columbus, OH 43210

Abstract

Although the inositol phosphatase SHIP-1 is generally thought to inhibit signaling for Fc receptor-mediated phagocytosis, the product of its activity, phosphatidylinositol 3,4 bisphosphate ($PI(3,4)P_2$) has been implicated in activation of the NADPH oxidase. This suggests that SHIP-1 positively regulates generation of reactive oxygen species after phagocytosis. To examine how SHIP-1 activity contributes to Fc receptor-mediated phagocytosis, we measured and compared phospholipid dynamics, membrane trafficking and the oxidative burst in macrophages from SHIP-1-deficient and wild-type mice. SHIP-1-deficient macrophages showed significantly elevated ratios of PI(3,4,5) P_3 to $PI(3,4)P_2$ on phagosomal membranes. Imaging reactive oxygen intermediate activities in phagosomes revealed decreased early NADPH oxidase activity in SHIP-1-deficient macrophages. SHIP-1-deficiency also altered later stages of phagosome maturation, as indicated by the persistent elevation of PI(3)P and the early localization of Rab5a to phagosomes. These direct measurements of individual organelles indicate that phagosomal SHIP-1 enhances the early oxidative burst through localized alteration of the membrane 3′ phosphoinositide composition.

INTRODUCTION

The formation and maturation of phagosomes are regulated by membrane phospholipids (1). 3′ phosphoinositides generated early during phagocytosis regulate closure of the phagocytic cup (2). The activities of Type III phosphatidylinositol 3-kinase (PI3K), forming PI(3)P, contribute to later signals for phagosome maturation (3–6). Lipid phosphatases play key inhibitory roles in Fc receptor (FcR)-mediated phagocytosis by modifying phosphoinositides present on the phagosomal membrane. During phagocytosis, phosphoinositide concentrations change dramatically on phagosomal membranes, and disruption of phosphoinositide dynamics can alter phagocytosis (7–9).

The inositol phosphatase Src homology 2 domain-containing inositol phosphatase-1 (SHIP-1) inhibits phagocytosis and signaling in cells of the hematopoietic lineage (10). In macrophages, SHIP-1 is recruited via its SH2 domain to the phosphorylated immunoreceptor tyrosine-based activating motifs (ITAMs) and immunoreceptor tyrosine-

[1]Work supported by NIH Grants AI35950 and AI64668 to J.S. and NCI P01 CA095426 to S.T.

based inhibitory motifs (ITIMs) in the cytoplasmic tails of activating and inhibitory FcRs (11–13). Upon recruitment to FcRs, SHIP-1 is activated by phosphorylation, possibly via a Src family kinase (14). This membrane-associated, active SHIP-1 dephosphorylates phosphatidylinositol 3,4,5 trisphosphate, [PI(3,4,5)P_3], yielding phosphatidylinositol 3,4 bisphosphate, [PI(3,4)P_2] (15).

SHIP-1 inhibits many receptor-mediated signaling processes. In activated B cells, SHIP-1 recruitment to FcγRIIb decreases levels of PI(3,4,5)P_3 on the plasma membrane, consequently decreasing Ca^{2+} flux by inhibiting signaling via Bruton's tyrosine kinase (Btk) and phospholipase C (PLC) γ (16,17). Mice deficient in SHIP-1 expression die young from splenomegaly and extensive myeloid infiltration of the lungs (18), with decreased levels of B cell precursors, increased B cell proliferation and resistance of B cells to BCR-mediated death, mostly resulting from increased Akt phosphorylation (19,20). Macrophages from SHIP-1-deficient mice exhibit enhanced rates of phagocytosis (13), increased Rac activity, Erk phosphorylation, production of inflammatory cytokines IL-1β and IL-6, and NADPH oxidase activation (21). Thus, SHIP-1 is generally thought to inhibit signaling from receptors.

FcR-mediated phagocytosis is usually accompanied by assembly and activation of the NADPH oxidase complex (NOX2) on the phagosomal membrane, generating reactive oxygen intermediates (ROI) in the lumen of the compartment (22). The NADPH oxidase is comprised of six components: $p40^{phox}$, $p47^{phox}$, $p67^{phox}$, Rac, $p22^{phox}$ and $gp91^{phox}$. Upon stimulation, active complex is generated by translocation of the cytosolic $p40^{phox}$, $p47^{phox}$, $p67^{phox}$ and Rac2 to the plasma membrane or phagosomal membrane, where cytochrome b_{558} ($gp91^{phox}$ and $p22^{phox}$) is located, or delivered separately by vesicle-mediated trafficking (22). Once in complex with $gp91^{phox}$, $p67^{phox}$ and Rac2 stimulate electron flow through cytochrome b_{558} (23,24), oxidizing NADPH and reducing O_2 to superoxide.

The proteins $p40^{phox}$ and $p47^{phox}$ regulate NOX2 through direct or indirect interactions with 3′ phosphoinositides (3′PIs). Recruitment of both proteins to phagosome membranes is necessary for activation of NOX2 in response to FcR ligation (25–27). $p40^{phox}$ and $p47^{phox}$ contain PX domains that bind to PI(3)P and PI(3,4)P_2, respectively (28). Inhibition of PI3K through wortmannin treatment inhibits the oxidative burst in neutrophils (29). The $p40^{phox}$–dependent activation of NOX2 during Fc receptor-mediated phagocytosis requires the presence of PI(3)P on phagosome membranes(26,30). In addition, $p47^{phox}$ translocation to the phagosome membrane is preceded by its phosphorylation by protein kinase C (PKC), which may itself be regulated by PI(3,4,5)P_3 or PI(3,4)P_2 (31–35). However, although SHIP-1 might be expected to augment phagosomal ROI generation by increasing levels of PI(3,4)P_2, measurements of ROI after phagocytosis in $SHIP1^{-/-}$ macrophages indicated that SHIP-1 inhibits the oxidative burst (21).

Detection of subtle changes in signaling often requires direct observation of activities in individual cells. Previous work has shown that PH domains fused to fluorescent proteins can be used as probes for specific phosphoinositides. The PH domain of Plcδ1, which binds to PI(4,5)P_2, and the PH domain of Akt, which binds to both PI(3,4,5)P_3 and PI(3,4)P_2, have been used to trace the dynamics of their cognate phosphoinositides during phagocytosis (7). In addition, a fluorescent chimera of the tandem FYVE domain from Hrs (2xFYVE) has been used to visualize PI(3)P on phagosomes (36). Quantitative fluorescence microscopy of macrophages expressing fluorescent PH domain chimeras allowed us to analyze the dynamics of 3′PIs and the enzymes that control their formation during FcR-mediated phagocytosis (37). A SHIP1-YFP chimera revealed that SHIP-1 is recruited during the initiation of phagocytosis, then dissociates from the phagosome, redistributing to the

cytosol. The transient association of SHIP-1 on the phagosome suggested that its activities contribute positively to phagosome formation or to early changes in phagosome identity.

Because of the important roles for 3′ PIs in NOX2 activation and organelle trafficking, we hypothesized that SHIP-1 transiently increases $PI(3,4)P_2$ on phagosomes, with attendant increases in early NOX2 activity. Using quantitative fluorescence microscopy of bone marrow-derived macrophages from wild-type and SHIP1-deficient mice, we measured the timing and extent of early oxidative burst, the dynamics of $PI(3,4,5)P_3$, $PI(3,4)P_2$ and PI(3)P, as well as other markers of phagosome formation and maturation. Our results indicate an early positive role for SHIP-1 in the FcR-stimulated activation of NOX2.

MATERIALS AND METHODS

Molecular Cloning and DNA Manipulation

Plasmids encoding monomeric versions (A207K) of cyan fluorescent protein (CFP), citrine (CIT) (38), and yellow fluorescent protein (YFP), were used where indicated. β-actin from pEYFP.actin.c1 (Clontech, Mountainview, CA) was transferred into the pmCherry.C1 vector expressing monomeric Cherry (Roger Tsien, University of California San Diego, San Diego, CA). The PH domains of human PLCδ1 and Bruton's tyrosine kinase (Btk) were gifts from Tamas Balla (39,40). The PLCδ1PH construct was PCR amplified, adding Xho1 and BamH1 restriction sites, and subcloned into pmCitrine-N1 (Clontech). The BtkPH construct was PCR amplified and subcloned into the pmCitrine-N1 vector between Xho1 and HindIII. Human Tapp1 constructs were obtained from MRC (Protein Phosphorylation Unit Dundee, Scotland) and the C-terminal PH domain was subcloned into pmCitrine-C1 or pmCFP-C1 at the EcoR1-BamH1 site. GFP-LAMP-1 was provided by Norma Andrews (Yale University School of Medicine, New Haven, CT) and cloned into pEYFP-N1 between EcoR1 and BamH1 (Clontech). GFP-2xFYVE, the tandem FYVE finger domains from hepatocyte growth factor-regulated tyrosine kinase substrate (Hrs), a gift of Harald Stenmark (Norwegian Radium Hospital, Oslo, Norway), was cloned into pmCitrine.C1 and pmCherry.C1 between HindIII and Kpn1 (Clontech). GFP-Rab5a, provided by Philip Stahl (Washington University, St. Louis, MO), was cloned into pmCitrine.C1 between HindIII and BamH1. Rab7 cDNA was a gift from Angela Wandinger-Ness (University of New Mexico, Albuquerque, NM) and cloned into pEYFP-C1 between Xho1 and Kpn1 (Clontech) (41). All DNA sequences were confirmed at the University of Michigan DNA Sequencing Core.

Tissue Culture and Transfection

Bone marrow-derived macrophages (BMDMs) were obtained from femurs of $SHIP1^{-/-}$ mice and age-matched wild-type littermates (18). The cells were cultured for 5–8 days as previously described (42). BMDMs were prepared for ratiometric microscopy by harvesting in cold phosphate-buffered saline (PBS) and counted. Alternatively, BMDMs that had been frozen on Day 6 of culture were thawed and counted. Using the Amaxa Nucleofector system kit for mouse macrophages, $\sim 1\times10^6$ cells were transfected per condition; they were divided evenly among three 25 mm coverslips and cultured overnight in RPMI with 20% h.i. FBS, 20 U/mL penicillin, and 20 μg/mL streptomycin, as described in the manufacturer's protocol (VPA-1009, Amaxa Biosystems, Cologne, Germany,).

RAW264.7 cells (RAWs), a murine macrophage-like cell line (American Type Culture, Manassas, VA) were cultured at 37°C with 5% CO_2. RAWs were cultured in Advanced-DMEM with 2% heat inactivated (h.i.) fetal bovine serum, 4 mM L-glutamine, 20 U/mL penicillin, and 20 μg/mL streptomycin using Invitrogen cell culture reagents (Carlsbad, CA). RAWs were prepared for ratiometric microscopy by plating $\sim 2.5\times10^5$ cells per coverslip the

day before imaging. After cells had attached to the coverslip (~3 hours), cells were transfected with plasmids encoding the fluorescent chimeras, using Roche FuGene-6 as described in the manufacturer's protocol (Roche Diagnostics, Indianapolis, IN).

For microscopy, coverslips with cells were assembled into Leiden chambers (Harvard Apparatus, Holliston, MA) at 37°C in Ringer's buffer (155 mM NaCl, 5 mM KCl, 2 mM $CaCl_2$, 1 mM $MgCl_2$, 2 mMNaH_2PO_4, 10 mM glucose, 10 mM HEPES at pH 7.2). Sheep erythrocytes (Lampire Biological Laboratories, Pipersville, PA) were opsonized with IgG and added to the macrophages as previously described (43).

Ratiometric Microscopy

Ratiometric images were acquired on an inverted fluorescence microscope (Nikon TE300) with a 60x N.A.1.4 Planapo objective, a mercury arc lamp as the light source for epifluorescence imaging and a cooled digital CCD camera (Quantix; Photmetrics). The microscope was equipped with a temperature-controlled stage, filter wheels and shutters for both excitation and emission filters (Lambda 10-2 filter wheel controller, Sutter Instruments), and dichroic mirrors that allow detection of multiple fluorophores via a JP4v2 filter set (Chroma Technology, Rockingham, VT). All images were acquired and processed using Metamorph 6.2r6 (Universal Imaging, Malvern, PA).

After delivering ~2×10^5 IgG-opsonized erythrocytes to the target area of the coverslip BMDMs expressing fluorescent proteins were observed undergoing phagocytosis. Upon landing of an erythrocyte on a macrophage, CIT/YFP (selected by the same filters), CFP and phase-contrast images were recorded every fifteen seconds until completion of phagocytosis (~10 minutes). The ratio image (R_M) was then calculated, representing the molar ratio of CIT chimera to CFP at every pixel in the cell.

To generate molar ratio images based upon stoichiometric FRET methods (44), chimeric CIT was expressed with soluble CFP, which served as a marker of cell thickness. The ratio image, R_M, was calculated assuming that there was no FRET between the fluorescent molecules:

$$R_M = \left(\frac{\xi}{\gamma}\right)\frac{\alpha I_A}{I_D}.$$

Where I_A corresponds to the CIT or YFP image (excitation 505 nm, emission 540 nm) and I_D corresponds to the CFP image (excitation 435 nm, emission 490 nm). When two chimeras were expressed together, it could not be possible assumed that there would be no FRET. Therefore, the ratio was calculated as follows:

$$R_M = \frac{[\text{Acceptors Total}]}{[\text{Donors Total}]} = \left(\frac{\xi}{\gamma}\right)\frac{\alpha I_A}{(I_F - \alpha I_A - \beta I_D)\xi + I_D}$$

Where I_F corresponds to the FRET image (excitation 435 nm, emission 540 nm). The FRET coefficents α, γ and ξ were calculated from calibrating the microscope with a series of images from cells transfected with CFP, citrine or a linked CFP-citrine chimera with known FRET efficiency (44). Shading-correction images were taken by imaging solutions of CFP and CIT sandwiched between two coverslips.

Comparative studies determined that although phagocytosis occurred more quickly in BMDM than in RAW 264.7 macrophages, the overall patterns of phosphoinositide dynamics

were similar. Using CIT-chimera probes for $PI(4,5)P_2$ (Plcδ1PH), $PI(3,4,5)P_3$ (BtkPH), $PI(3,4)P_2$ (TappPH), and PI(3)P (2xFYVE), the time of maximal amplitude for each probe was measured and plotted relative to phagosomal cup formation and closure. Comparing the dynamics of 3′PIs in BMDM with those observed in previous studies of RAW 264.7 cells, we found that in both cells, $PI(4,5)P_2$, $PI(3,4,5)P_3$, and $PI(3,4)P_2$ peaked on phagosomal membranes before phagosome closure and PI(3)P peaked 1–2 mins after closure (data not shown).

Particle Tracking

Recruitment of YFP chimeras to phagosomes was measured using the particle-tracking algorithm TRACKOBJ in Metamorph. As previously described, a 5 μm region was drawn on the target erythrocyte, allowing it to be tracked as it was internalized into the macrophage (45). For every frame in a stack of images comprising a movie, we computed R_M in the cell (R_C) and R_M in the phagosome (R_P), producing the recruitment index R_P/R_C.

To align multiple phagocytic events from different time-lapse sequences, a circular region was drawn over the phase-contrast image, marking where the erythrocyte would contact the cell. The beginning of pseudopod extension and cup formation was identified as the first frame in the sequence with an increase in CFP fluorescence inside the circular region. Multiple phagocytic image series were then aligned for analysis based on that operational definition of time-point zero.

Oxidative Burst

To measure the levels of reactive oxygen intermediates (ROI) produced during phagocytosis of IgG-opsonized erythrocytes, macrophages undergoing phagocytosis were stained with nitroblue tetrazolium (NBT) and fixed and counted for the amount of formazan converted. BMDMs were plated at a concentration of 2×10^5 cells per 13 mm coverslip and cultured overnight in DMEM with 10% heat-inactivated FBS in 24-well dishes. Cells were washed in cold PBS and resuspended in cold Ringer's Buffer containing a 20% saturated NBT solution (Sigma Aldrich, Saint Louis, MO) and IgG-opsonized erythrocytes at a ratio of 100:1. The erythrocytes were allowed to rosette on the cells for 10 minutes at 4°C. The macrophages were rinsed with warm DMEM containing a 20% saturated NBT solution and incubated for 45 minutes at 37°C, rinsed in ddH_2O allowing the uninternalized erythrocytes to lyse. The macrophages were washed 2x with cold PBS and then fixed with methanol. After methanol fixation, cells were counterstained with a 0.02% safranin solution (Sigma Aldrich, Saint Louis, MO). Cells were scored based upon the number of purple formazan positive phagosomes per 100 cells.

To prepare microspheres labeled with IgG and oxyburst, 3 μm-diameter amine polystyrene beads (Polysciences Inc., Warrington, PA) were incubated in 1 M sodium bicarbonate buffer pH 9.0 and 0.5 mg of Oxyburst H_2DCFDA succinimidyl ester (Molecular Probes, Eugene, OR, D-2935) for 2 hours at room temperature. Beads were washed two times in 1 M glycine/PBS and incubated for an additional 30 min at 37° in PBS with 0.25 mg/mL rabbit IgG. Beads were washed three times in 0.1% BSA and then added to the macrophages.

To measure oxidase activity during phagocytosis, wild-type or SHIP-1-deficient macrophages were plated onto 25 mm coverslips, in RPMI 1640 with 20% h.i. FBS, following transfection with plasmids for actin-mCherry, and incubated overnight. Fluorescence excitation and emission wavelengths were selected via a Texas Red/FITC filter set (Omega Optical, Brattleboro, VT). Actin-positive cells were imaged after addition of Oxyburst-IgG beads. Images were collected every minute for 30 minutes, using the FITC filter for Oxyburst (excitation 492 nm, emission 535 nm) and the RFP filter for actin-

mCherry (excitation 572 nm, emission 630 nm) images. The value of Oxyburst fluorescence was quantitated by measuring the average fluorescence intensity in the region of the internalized bead. Events were synchronized by the first movement of actin (as indicated by a rise in Texas Red fluorescence) into the phagosomal area. The average rise in Oxyburst fluorescence was measured over time.

To compare PI(3)P formation and oxidase activity, BMDM were plated onto 25 mm coverslips as previously described and transfected with plasmids for mCFP and 2xFYVE-mCherry. Following overnight incubation, the cells were imaged. Fluorescence excitation and emission wavelengths were selected via a CFP/YFP/RFP filter set (Chroma Technology, Rockingham, VT). 2xFYVE-mCherry, CFP-positive cells were imaged after the addition of Oxyburst-IgG beads. Images were collected every minute for 30 minutes, using the RFP filter for 2xFYVE-mCherry (excitation 572 nm, emission 630 nm), the CFP filter for CFP (excitation 435 nm, emission 490 nm) and the YFP filter for Oxyburst (excitation 505 nm, emission 540 nm). The increase in Oxyburst (YFP) and 2xFYVE (mCherry) fluorescence was measured by calculating the average fluorescence intensity in the region of the internalized bead and dividing that by the corresponding fluorescence intensity of untagged CFP in the same region. The ratio in the phagosome, R_P, and the ratio in the cell, R_C, were calculated over time and plotted as R_P/R_C. Thus, a rise in the R_P/R_C value over a baseline value of 1.0 indicated oxidase activation for the YFP ratio to CFP and formation of PI(3)P for the mCherry ratio.

Statistical Analysis

All statistical analysis was conducted using the Students T-test, assuming unequal variances. Data more than 2 standard deviations from the mean were excluded from the analysis, with the exception of Fig. 4B.

RESULTS

Alteration of Phosphoinositide Dynamics by SHIP-1

BMDM from SHIP-1-deficient mice or their wild-type littermates were used to analyze the effect of SHIP-1 upon 3′ PI dynamics and signaling during FcR-mediated phagocytosis. BMDM were transfected with soluble CFP and either YFP chimeras of actin or CIT chimeras of PH domain probes for $PI(4,5)P_2$, $PI(3,4,5)P_3$ or $PI(3,4)P_2$. Fluorescence images were collected from cells during phagocytosis, and the molar ratio, R_M, between the CIT chimera and CFP was calculated for each pixel of the cell image, using FRET stoichiometry (44). Recruitment of YFP or CIT chimeras to phagosomes was quantified by dividing the average R_M on the phagosome (R_P) by the average R_M of the entire cell (R_C); R_P/R_C values greater than one indicated recruitment (9,37). Images from multiple video sequences were aligned and compared quantitatively (Fig. 1). To compare the time course of phagocytosis between the wild-type and SHIP-$1^{-/-}$ macrophages, we measured the dynamics of β actin-YFP during phagocytosis between the two populations of cells (Fig. 1A). Although previous work showed that SHIP-1-deficient macrophages exhibit enhanced rates of phagocytosis (13,46), we detected no significant difference in the actin dynamics during the early stages of phagocytosis (Fig. 1A). Analyses of rates of phagocytosis in phase-contrast microscopic time series, measured from the beginning of cup formation to closure of the phagosome, also indicated similar rates for wild-type and mutant macrophages (WT = 3.75 ± 0.34 min, n=14; $SHIP^{-/-}$ = 3.32 ± 0.30 min, n=10; $p > 0.35$). Previous studies compared rates of phagocytosis between wild-type and $SHIP1^{-/-}$ macrophages by measuring the number of particles ingested after various intervals of incubation with particles. Using similar methods, we also found that SHIP-1-deficient macrophages ingested more particles at early time points of phagocytosis (data not shown). The different results from different assays may be

reconciled if wild-type and SHIP1$^{-/-}$ macrophages ingest at similar rates but SHIP-1-deficiency lifts a restraint on the macrophage's ability to initiate phagocytosis in rapid succession.

The dynamics of PI(4,5)P_2 were examined in macrophages from SHIP-1-deficient and wild-type mice, as approximated by the localization patterns of Plcδ1PH-CIT. PI(4,5)P_2 dynamics in SHIP1$^{-/-}$ macrophages exhibited decreased levels of Plcδ1PH-CIT during cup formation (Fig 1B). The SHIP-1 substrate PI(3,4,5)P_3 was localized using BtkPH-CIT. Small but statistically insignificant increases of PI(3,4,5)P_3 were detected on phagosomal membranes in SHIP1$^{-/-}$ macrophages, compared to wild-type (Fig. 1C). The product of SHIP-1 activity, PI(3,4)P_2, was localized using Tapp1PH-CIT. We observed a small but insignificant decrease of PI(3,4)P_2 on the phagosomal membranes of SHIP1$^{-/-}$ macrophages (Fig. 1D). The high levels of Tapp1PH-CIT recruitment to phagosomes of SHIP1$^{-/-}$ macrophages indicated roles for other enzymes in generating PI(3,4)P_2, such as Type I PI 3-kinase and SHIP-2 (47,48).

The insignificant changes in substrate and product detected in the absence of SHIP-1 indicates either a lack of sensitivity in the microscopic method or an inherent variability in phosphoinositide dynamics on individual phagosomes. We postulated that measuring the ratio of substrate to product on each phagosome might provide a more sensitive method of detecting effects of SHIP-1 on levels of its substrate and product. Therefore, we expressed BtkPH-CIT and TappPH-CFP in macrophages from SHIP1$^{-/-}$ and wild-type mice and measured R_M during phagocytosis (Fig. 1E). The ratio of BtkPH-CIT to TappPH-CFP was elevated in phagosomes of SHIP1$^{-/-}$ macrophages, indicating that SHIP-1 increases the ratio of PI(3,4)P_2 to PI(3,4,5)P_3 on phagosomal membranes. This modest but significant change in 3′ phosphoinositide levels may influence later activities, such as the oxidative burst or phagosome maturation.

SHIP-1 Increases Early NOX2 Activity on Phagosomes

To determine if SHIP1 affects ROI levels during phagocytosis, wild-type or SHIP1$^{-/-}$ macrophages expressing actin-mCherry were imaged during phagocytosis of polystyrene beads labeled with IgG and Oxyburst (H_2DCFDA, dichlorohydrofluorescein diacetate) succinimidyl ester (Fig. 2). Following phagocytosis, bead fluorescence increased as Oxyburst was reduced to dichlorofluorescein (Fig. 2A, Suppl. Movie 1). Almost immediately after phagosome closure, oxyburst fluorescence appeared on the beads (Fig. 2A). This effect was much more pronounced in phagosomes of wild-type BMDM. To analyze the fluorescence conversion quantitatively, separate image series were synchronized using the frame with images showing the first detectable movement of actin-mCherry over the phagosome. Quantitative measurements of fluorescence showed that, compared to wild-type macrophages, SHIP1$^{-/-}$ macrophages generated both a lower maximum fluorescence and a delayed time to peak fluorescence, (Figs. 2B, C).

These results differ from previous reports that indicated SHIP-1 deficiency increased the oxidative burst (21). In those studies, however, oxidase activity was measured two hours after initiation of phagocytosis. The Oxyburst beads were not useful for comparing late times after phagocytosis. To examine superoxide production over a longer interval, wild-type or SHIP1$^{-/-}$ macrophages were stained with Nitroblue tetrazolium (NBT). In the presence of superoxide, NBT is converted to formazan, which appears by bright-field microscopy as a purple stain in the phagosome (49). Macrophages were fixed after undergoing phagocytosis for 45 minutes and the number of stained phagosomes per 100 macrophages were scored. After 45 minutes of phagocytosis, SHIP1$^{-/-}$ macrophages showed a significant increase in the amount of formazan-positive phagosomes, indicating increased superoxide production (WT = 51.3 NBT+ phagosomes/100 cells, SHIP1$^{-/-}$ = 87.9

NBT+ phagosomes/100 cells, p-value < 0.005). Independent measurements ensured that the increase in superoxide-positive phagosomes was not due to increased numbers of phagosomes in SHIP1$^{-/-}$ macrophages (data not shown). Therefore, SHIP-1 deficiency decreased ROI generation during early stages of phagocytosis, as measured by oxyburst conversion, and increased it at later times, as measured by NBT conversion. Technical limitations prevented the application of a single method for comparing early and late responses.

To examine whether SHIP-1 effects on oxyburst conversion were related to phagosomal PI(3)P dynamics, we monitored PI(3)P in macrophages expressing fluorescent 2xFYVE. In BMDM expressing 2xFYVE-YFP and free CFP, the 2xFYVE domain localized to small intracellular vesicles (Fig. 3), as observed previously in RAW macrophages (9). Upon internalization of opsonized erythrocytes, 2xFYVE-YFP fluorescence increased on the phagosomes of both wild-type and SHIP1$^{-/-}$ macrophages (Fig. 3A). To compare the patterns of PI(3)P formation and oxidase activation during FcR-mediated phagocytosis, wild-type macrophages expressing 2xFYVE-mCherry and free CFP were fed oxyburst-coated, IgG-opsonized polystyrene beads. Imaging revealed that 2xFYVE-mCherry recruitment to nascent phagosomes preceded conversion of oxyburst (Fig. 3B). From time-lapse sequences of phagocytosis, we measured the ratios of 2xFYVEmCherry to CFP and oxyburst (YFP) to CFP and compared the R_P/R_C levels over time (Fig. 4A). These measurements indicated that the increase in PI(3)P preceded or coincided with the fluorogenic conversion of oxyburst on beads (Fig. 4A). Quantitative analysis of macrophages expressing 2xFYVE-YFP and CFP indicated that rates of PI(3)P generation were similar on wild-type and SHIP1$^{-/-}$ phagosomes (Fig. 4B). This suggests that PI(3)P contributes to early generation of ROI on phagosomes. Furthermore, the decreased generation of ROI in phagosomes of SHIP1$^{-/-}$ macrophages was not due to a deficiency in PI(3)P generation.

Although rapid increases in PI(3)P were detected in both wild-type and SHIP1$^{-/-}$ phagosomes, the levels of PI(3)P reached higher levels, and remained elevated longer, in SHIP1$^{-/-}$ macrophages (Fig. 4B). The higher levels of PI(3)P on phagosomes of SHIP1$^{-/-}$ macrophages suggested that SHIP-1 activities affect phagosome maturation. Previous work has shown that PI(3)P facilitates the recruitment of different signaling proteins to early and late endosomes. Rab5a, an early endosome marker, is recruited to membranes containing PI(3)P, where it is thought to stimulate the formation of additional PI(3)P (50,51). Rab7 localizes to vesicles containing PI(3)P and to late endosomes (9,41,52). Lysosome-associated membrane protein-1 (Lamp-1) localizes to late endosomes and lysosomes (9,53). To measure early stages of maturation, phagosomal Rab5a-CIT was expressed with free CFP and the amount of the Rab5a chimera localized to the phagosomal membrane was calculated. Rab5a-CIT increased significantly during the later stages of phagocytosis in SHIP1$^{-/-}$ macrophages (Fig. 5A). To examine later stages of phagosome maturation, we measured the association of Rab7-YFP and Lamp1-YFP with phagosomes. Rab7 levels were significantly decreased in SHIP1$^{-/-}$ macrophages during the early stages of cup formation and closure (Fig. 5B). However, Rab7 peaked at similar levels in both macrophage populations. The formation of phagolysosomes, as measured by localization of Lamp1-YFP to the phagosomes, was also significantly altered in SHIP1$^{-/-}$ macrophages (Fig. 5C). As the phagosome matured, Lamp-1 levels on the surface of the SHIP1$^{-/-}$ macrophages were increased above that seen in wild-type macrophages. However, peak values of Lamp-1 levels on the phagosomes were not significantly different between the two genotypes. Thus, SHIP-1-deficiency altered the dynamics of phagosome maturation, most likely through its effects on phagosomal levels of 3′PIs.

DISCUSSION

This study demonstrates that SHIP-1 activity in macrophages modulates 3′ phosphoinositide dynamics on phagosomes, with consequent effects on the early oxidative burst and the kinetics of phagosome maturation. This indicates that the enzyme is not simply inhibiting phagocytic signals, but also providing positive signals. Most notably, SHIP-1 increased the ratio of $PI(3,4)P_2$ to $PI(3,4,5)P_3$ on the phagosomal membranes and increased early generation of ROI on phagosomes. This is consistent with a role for 3′ phosphoinositides in coordinating the activation of NOX2 during phagocytosis.

The differences in 3′ phosphoinositide levels on phagosomes were subtle. When the levels of the SHIP-1 substrate, $PI(3,4,5)P_3$ or product, $PI(3,4)P_2$ were measured separately, small but insignificant differences were detected between wild-type and mutant cells. However, when we measured substrate and product in the same cells, $SHIP1^{-/-}$ macrophage phagosomes contained significantly higher ratios of $PI(3,4,5)P_3$ to $PI(3,4)P_2$. Measuring the ratio of product and substrate on individual phagosomes increased the sensitivity of the system and allowed detection of SHIP-1 effects on $PI(3,4,5)P_3$ and $PI(3,4)P_2$ levels during phagocytosis. The small differences in ratio do not necessarily indicate that the contribution of SHIP-1 is slight. Ratiometric fluorescence microscopy measures the relative redistribution of the chimeras from an initially uniform distribution in cytoplasm. The magnitudes of changes in R_P/R_C will be affected by the variation in the magnitudes of 3′PI responses, by probe expression levels and by probe affinities for 3′PIs. Low changes in ratios could result if a low binding affinity of BtkPH for $PI(3,4,5)P_3$ underestimates the actual changes in $PI(3,4,5)P_3$ concentrations on phagosomes or if a high binding affinity of Tapp1PH for $PI(3,4)P_2$ underestimates the actual changes in $PI(3,4)P_2$ concentrations. It also remains possible that the principal effect of SHIP1 depletion is on the ratio of $PI(3,4,5)P_3$ to $PI(3,4)P_2$, rather than the absolute level of $PI(3,4)P_2$ available for oxidase activation. A change in ratio could affect the recruitment of $p47^{phox}$ and the activation of the oxidase.

Our findings are at odds with published observations of 3′PI dynamics in $SHIP1^{-/-}$ neutrophils. When exposed to chemoattractants, the $SHIP1^{-/-}$ neutrophils exhibit diffuse localization of the Akt PH domain, a proxy for both $PI(3,4,5)P_3$ and $PI(3,4)P_2$. Actin polymerization is also impacted, showing a disorganized polymerization (54). We did not observe a similar defect in actin polymerization or $PI(3,4,5)P_3$ and $PI(3,4)P_2$ dynamics during FcR-mediated phagocytosis, but this may be attributable to differences in the signal transduction pathways controlling actin and phosphoinositides during chemotaxis.

Compared to SHIP-1-deficient macrophages, wild-type macrophages showed stronger oxidative burst early, but diminished activity overall. The observation that $SHIP1^{-/-}$ macrophages produced significantly less ROI early during phagocytosis indicates that increased levels of $PI(3,4)P_2$ on phagosomes augment NOX2 activity. Previous work has shown that NOX2 can be activated by PI(3)P (30) and, in permeabilized neutrophils, by $PI(3,4,5)P_3$ or $PI(3,4)P_2$ (34). Possible mechanisms for this are suggested by biochemical studies. $p47^{phox}$ binds to both $PI(3,4,5)P_3$ and $PI(3,4)P_2$, allowing its translocation to intracellular membranes (22,28,32). In permeabilized neutrophils, PKCδ is activated by both $PI(3,4,5)P_3$ and $PI(3,4)P_2$ and can phosphorylate $p47^{phox}$ (34,35). SHIP-1 facilitates the oxidative burst *in vitro* with GTP-γS-Rac, $p67^{phox}$, $p47^{phox}$, and neutrophil membranes (55). Our measurements of PI(3)P and oxyburst conversion on phagosomes indicated that SHIP-1 does not affect early increases in PI(3)P levels (Figs 3, 4), which suggests that the increased ROI in wild-type macrophage phagosomes relates to their higher levels of $PI(3,4)P_2$.

The different effects of SHIP-1-deficiency on ROI generation suggest that NOX2 is regulated by 3′PIs in two different ways. The early oxidative burst may be enhanced by

SHIP-1-generated PI(3,4)P_2 on the phagosome. In contrast, the later oxidative burst may be more dependent upon levels of PI(3)P. SHIP-1 deficiency increased levels of PI(3)P, leading to increased oxidase activity during the later stages of phagosome maturation. It is possible that the oxidative burst takes place in two sequential phases, the first dependent on both PI(3,4)P_2 and PI(3)P and the second more dependent on PI(3)P. The increased ROI generation by SHIP1−/− macrophages at later time points may reflect the increased levels of PI(3)P persisting on phagosomes in those macrophages.

Although the effects of SHIP-1 deficiency upon its substrate and product were subtle, the effects on phagosomal PI(3)P levels were more pronounced. Previous work has shown that SHIP-1 is present on phagosomal membranes early but redistributes back to the cytosol after phagosomal closure (37,56). These early SHIP-1 activities may bias subsequent phagosome formation and maturation. Accordingly, the difference observed in PI(3)P on fully formed phagosomes would be set up by activities occurring while SHIP-1 is membrane-associated. It is possible that levels of a substrate in the phagosomal cup are modulated by SHIP-1 activity, and that this action limits the amount of PI(3)P generated during the later stages of phagocytosis.

The striking persistence of PI(3)P on phagosomes in the SHIP1$^{-/-}$ macrophages could underlie the observed alterations in endocytic trafficking. Alternatively, it is possible that early oxidase activity may affect the subsequent maturation of the phagosome, and that SHIP-1 may affect maturation indirectly by stimulating the oxidative burst. Expression of CIT or YFP-tagged chimeras of Rab5a for early endosomes, Rab7 for late endosomes, and Lamp-1 for late endosomes and lysosomes(9,57) allowed comparisons of phagosome maturation in SHIP1$^{-/-}$ and wild-type macrophages. Initially, both populations of macrophages had similar levels of Rab5a on their phagosomes, but levels of Rab5a continued to increase on phagosomes in SHIP1$^{-/-}$ macrophages. From cup formation to the late stages of phagocytosis (30 minutes), Rab7 levels were lower and Lamp-1 levels were higher on SHIP1$^{-/-}$ phagosomes; however, both Rab7 and Lamp-1 peaked at similar values in both populations of macrophages. These differences in the later stages of phagosome maturation could be interpreted two ways. Either SHIP-1 is altering endocytic trafficking, or the observed differences are due to limitations in the sensitivity of ratiometric microscopy. The membrane markers Rab7, Rab5a, and Lamp-1 are distributed in a punctate pattern in the interior of the cell, where they label the intracellular vesicles. When a phagosome is initially formed, the perinuclear concentration of these probes excludes them from the forming phagosome, creating low R_P/R_C values. As the phagosome merges with the intracellular vesicles during maturation, R_P/R_C values then rise. Differences in the initial distributions of the chimeras, between wild-type and SHIP-1 macrophages, could account for different starting levels observed on the forming phagosome with Rab7 and Lamp-1.

Two pathways to PI(3)P formation have been described in fibroblasts: PI3K-dependent phosphorylation of PI and dephosphorylation of PI(3,4,5)P_3 by 5′ and 4′ inositol phosphatases. Rab5a stimulates the activity of all three enzymes (51). The present finding that SHIP-1 activity impacted PI(3)P levels more than those of its substrate and product indicates a link between proximal signals related to FcR ligation and the Type III PI3K pathway of 3′PI generation in FcR-mediated phagocytosis. However, it remains possible that the effects of SHIP-1 deficiency on phagosome maturation result from SHIP-1 interactions with proteins necessary for membrane trafficking.

Supplementary Material

Refer to Web version on PubMed Central for supplementary material.

Acknowledgments

We thank Drs. Adam Hoppe, Ariel Savina and Peter Beemiller, for advice, Gerald Krystal, for the contribution of the SHIP1$^{-/-}$ mice, Latha Ganesan, for help in obtaining BMDM and Morton Brown, for advice about statistical analyses.

References

1. De Matteis MA, Godi A. PI-loting membrane traffic. Nat Cell Biol 2004;6:487–492. [PubMed: 15170460]
2. Araki N, Johnson MT, Swanson JA. A role for phosphoinositide 3-kinase in the completion of macropinocytosis and phagocytosis by macrophages. J Cell Biol 1996;135:1249–1260. [PubMed: 8947549]
3. Ellson CD, Anderson KE, Morgan G, Chilvers ER, Lipp P, Stephens LR, Hawkins PT. Phosphatidylinositol 3-phosphate is generated in phagosomal membranes. Curr Biol 2001;11:1631–1635. [PubMed: 11676926]
4. Schu PV, Takegawa K, Fry MJ, Stack JH, Waterfield MD, Emr SD. Phosphatidylinositol 3-kinase encoded by yeast VPS34 gene essential for protein sorting. Science 1993;260:88–91. [PubMed: 8385367]
5. Volinia S, Dhand R, Vanhaesebroeck B, MacDougall LK, Stein R, Zvelebil MJ, Domin J, Panaretou C, Waterfield MD. A human phosphatidylinositol 3-kinase complex related to the yeast Vps34p-Vps15p protein sorting system. Embo J 1995;14:3339–3348. [PubMed: 7628435]
6. Stephens L, Cooke FT, Walters R, Jackson T, Volinia S, Gout I, Waterfield MD, Hawkins PT. Characterization of a phosphatidylinositol-specific phosphoinositide 3-kinase from mammalian cells. Curr Biol 1994;4:203–214. [PubMed: 7922325]
7. Marshall JG, Booth JW, Stambolic V, Mak T, Balla T, Schreiber AD, Meyer T, Grinstein S. Restricted accumulation of phosphatidylinositol 3-kinase products in a plasmalemmal subdomain during Fc gamma receptor-mediated phagocytosis. J Cell Biol 2001;153:1369–1380. [PubMed: 11425868]
8. Botelho RJ, Teruel M, Dierckman R, Anderson R, Wells A, York JD, Meyer T, Grinstein S. Localized biphasic changes in phosphatidylinositol-4,5-bisphosphate at sites of phagocytosis. J Cell Biol 2000;151:1353–1368. [PubMed: 11134066]
9. Henry RM, Hoppe AD, Joshi N, Swanson JA. The uniformity of phagosome maturation in macrophages. J Cell Biol 2004;164:185–194. [PubMed: 14718518]
10. Damen JE, Liu L, Rosten P, Humphries RK, Jefferson AB, Majerus PW, Krystal G. The 145-kDa protein induced to associate with Shc by multiple cytokines is an inositol tetraphosphate and phosphatidylinositol 3,4,5-triphosphate 5-phosphatase. Proc Natl Acad Sci U S A 1996;93:1689–1693. [PubMed: 8643691]
11. Tridandapani S, Siefker K, Teillaud JL, Carter JE, Wewers MD, Anderson CL. Regulated expression and inhibitory function of Fcgamma RIIb in human monocytic cells. J Biol Chem 2002;277:5082–5089. [PubMed: 11741917]
12. Tridandapani S, Wang Y, Marsh CB, Anderson CL. Src homology 2 domain-containing inositol polyphosphate phosphatase regulates NF-kappa B-mediated gene transcription by phagocytic Fc gamma Rs in human myeloid cells. J Immunol 2002;169:4370–4378. [PubMed: 12370370]
13. Nakamura K, Malykhin A, Coggeshall KM. The Src homology 2 domain-containing inositol 5-phosphatase negatively regulates Fcgamma receptor-mediated phagocytosis through immunoreceptor tyrosine-based activation motif-bearing phagocytic receptors. Blood 2002;100:3374–3382. [PubMed: 12384440]
14. Tridandapani S, Kelley T, Pradhan M, Cooney D, Justement LB, Coggeshall KM. Recruitment and phosphorylation of SH2-containing inositol phosphatase and Shc to the B-cell Fc gamma immunoreceptor tyrosine-based inhibition motif peptide motif. Mol Cell Biol 1997;17:4305–4311. [PubMed: 9234687]
15. Drayer AL, Pesesse X, De Smedt F, Woscholski R, Parker P, Erneux C. Cloning and expression of a human placenta inositol 1,3,4,5-tetrakisphosphate and phosphatidylinositol 3,4,5-trisphosphate 5-phosphatase. Biochem Biophys Res Commun 1996;225:243–249. [PubMed: 8769125]

16. Bolland S, Pearse RN, Kurosaki T, Ravetch JV. SHIP modulates immune receptor responses by regulating membrane association of Btk. Immunity 1998;8:509–516. [PubMed: 9586640]
17. Scharenberg AM, El-Hillal O, Fruman DA, Beitz LO, Li Z, Lin S, Gout I, Cantley LC, Rawlings DJ, Kinet JP. Phosphatidylinositol-3,4,5-trisphosphate (PtdIns-3,4,5-P3)/Tec kinase-dependent calcium signaling pathway: a target for SHIP-mediated inhibitory signals. Embo J 1998;17:1961–1972. [PubMed: 9524119]
18. Helgason CD, Damen JE, Rosten P, Grewal R, Sorensen P, Chappel SM, Borowski A, Jirik F, Krystal G, Humphries RK. Targeted disruption of SHIP leads to hemopoietic perturbations, lung pathology, and a shortened life span. Genes Dev 1998;12:1610–1620. [PubMed: 9620849]
19. Brauweiler A, Tamir I, Dal Porto J, Benschop RJ, Helgason CD, Humphries RK, Freed JH, Cambier JC. Differential regulation of B cell development, activation, and death by the src homology 2 domain-containing 5′ inositol phosphatase (SHIP). J Exp Med 2000;191:1545–1554. [PubMed: 10790429]
20. Helgason CD, Kalberer CP, Damen JE, Chappel SM, Pineault N, Krystal G, Humphries RK. A dual role for Src homology 2 domain-containing inositol-5-phosphatase (SHIP) in immunity: aberrant development and enhanced function of b lymphocytes in ship−/− mice. J Exp Med 2000;191:781–794. [PubMed: 10704460]
21. Ganesan LP, Joshi T, Fang H, Kutala VK, Roda J, Trotta R, Lehman A, Kuppusamy P, Byrd JC, Carson WE, Caligiuri MA, Tridandapani S. FcgammaR-induced production of superoxide and inflammatory cytokines is differentially regulated by SHIP through its influence on PI3K and/or Ras/Erk pathways. Blood 2006;108:718–725. [PubMed: 16543474]
22. Babior BM. NADPH oxidase: an update. Blood 1999;93:1464–1476. [PubMed: 10029572]
23. Nisimoto Y, Motalebi S, Han CH, Lambeth JD. The p67(phox) activation domain regulates electron flow from NADPH to flavin in flavocytochrome b(558). J Biol Chem 1999;274:22999–23005. [PubMed: 10438466]
24. Diebold BA, Bokoch GM. Molecular basis for Rac2 regulation of phagocyte NADPH oxidase. Nature immunology 2001;2:211–215. [PubMed: 11224519]
25. Ellson CD, Davidson K, Ferguson GJ, O'Connor R, Stephens LR, Hawkins PT. Neutrophils from p40phox−/− mice exhibit severe defects in NADPH oxidase regulation and oxidant-dependent bacterial killing. J Exp Med 2006;203:1927–1937. [PubMed: 16880254]
26. Suh CI, Stull ND, Li XJ, Tian W, Price MO, Grinstein S, Yaffe MB, Atkinson S, Dinauer MC. The phosphoinositide-binding protein p40phox activates the NADPH oxidase during FcgammaIIA receptor-induced phagocytosis. J Exp Med 2006;203:1915–1925. [PubMed: 16880255]
27. Cross AR, Erickson RW, Curnutte JT. Simultaneous presence of p47(phox) and flavocytochrome b-245 are required for the activation of NADPH oxidase by anionic amphiphiles. Evidence for an intermediate state of oxidase activation. J Biol Chem 1999;274:15519–15525. [PubMed: 10336445]
28. Kanai F, Liu H, Field SJ, Akbary H, Matsuo T, Brown GE, Cantley LC, Yaffe MB. The PX domains of p47phox and p40phox bind to lipid products of PI(3)K. Nat Cell Biol 2001;3:675–678. [PubMed: 11433300]
29. Condliffe AM, Hawkins PT, Stephens LR, Haslett C, Chilvers ER. Priming of human neutrophil superoxide generation by tumour necrosis factor-alpha is signalled by enhanced phosphatidylinositol 3,4,5-trisphosphate but not inositol 1,4,5-trisphosphate accumulation. FEBS Lett 1998;439:147–151. [PubMed: 9849896]
30. Ellson C, Davidson K, Anderson K, Stephens LR, Hawkins PT. PtdIns3P binding to the PX domain of p40phox is a physiological signal in NADPH oxidase activation. Embo J 2006;25:4468–4478. [PubMed: 16990793]
31. Groemping Y, Lapouge K, Smerdon SJ, Rittinger K. Molecular basis of phosphorylation-induced activation of the NADPH oxidase. Cell 2003;113:343–355. [PubMed: 12732142]
32. Sumimoto H, Kage Y, Nunoi H, Sasaki H, Nose T, Fukumaki Y, Ohno M, Minakami S, Takeshige K. Role of Src homology 3 domains in assembly and activation of the phagocyte NADPH oxidase. Proc Natl Acad Sci U S A 1994;91:5345–5349. [PubMed: 8202490]

33. Leto TL, Adams AG, de Mendez I. Assembly of the phagocyte NADPH oxidase: binding of Src homology 3 domains to proline-rich targets. Proc Natl Acad Sci U S A 1994;91:10650–10654. [PubMed: 7938008]
34. Brown GE, Stewart MQ, Liu H, Ha VL, Yaffe MB. A novel assay system implicates PtdIns(3,4)P(2), PtdIns(3)P, and PKC delta in intracellular production of reactive oxygen species by the NADPH oxidase. Molecular cell 2003;11:35–47. [PubMed: 12535519]
35. Toker A, Meyer M, Reddy KK, Falck JR, Aneja R, Aneja S, Parra A, Burns DJ, Ballas LM, Cantley LC. Activation of protein kinase C family members by the novel polyphosphoinositides PtdIns-3,4-P2 and PtdIns-3,4,5-P3. J Biol Chem 1994;269:32358–32367. [PubMed: 7798235]
36. Gillooly DJ I, Morrow C, Lindsay M, Gould R, Bryant NJ, Gaullier JM, Parton RG, Stenmark H. Localization of phosphatidylinositol 3-phosphate in yeast and mammalian cells. Embo J 2000;19:4577–4588. [PubMed: 10970851]
37. Kamen LA, Levinsohn J, Swanson JA. Differential Association of Phosphatidylinositol 3-Kinase, SHIP-1, and PTEN with Forming Phagosomes. Mol Biol Cell. 2007
38. Zacharias DA, Violin JD, Newton AC, Tsien RY. Partitioning of lipid-modified monomeric GFPs into membrane microdomains of live cells. Science 2002;296:913–916. [PubMed: 11988576]
39. Varnai P, Balla T. Visualization of phosphoinositides that bind pleckstrin homology domains: calcium- and agonist-induced dynamic changes and relationship to myo-[3H]inositol-labeled phosphoinositide pools. J Cell Biol 1998;143:501–510. [PubMed: 9786958]
40. Varnai P, Rother KI, Balla T. Phosphatidylinositol 3-kinase-dependent membrane association of the Bruton's tyrosine kinase pleckstrin homology domain visualized in single living cells. J Biol Chem 1999;274:10983–10989. [PubMed: 10196179]
41. Stein MP, Feng Y, Cooper KL, Welford AM, Wandinger-Ness A. Human VPS34 and p150 are Rab7 interacting partners. Traffic (Copenhagen, Denmark) 2003;4:754–771.
42. Racoosin EL, Swanson JA. Macrophage colony-stimulating factor (rM-CSF) stimulates pinocytosis in bone marrow-derived macrophages. The Journal of experimental medicine 1989;170:1635–1648. [PubMed: 2681516]
43. Knapp PE, Swanson JA. Plasticity of the tubular lysosomal compartment in macrophages. J Cell Sci 1990;95(Pt 3):433–439. [PubMed: 2384523]
44. Hoppe A, Christensen K, Swanson JA. Fluorescence resonance energy transfer-based stoichiometry in living cells. Biophys J 2002;83:3652–3664. [PubMed: 12496132]
45. Hoppe AD, Swanson JA. Cdc42, Rac1, and Rac2 display distinct patterns of activation during phagocytosis. Mol Biol Cell 2004;15:3509–3519. [PubMed: 15169870]
46. Cox D, Dale BM, Kashiwada M, Helgason CD, Greenberg S. A regulatory role for Src homology 2 domain-containing inositol 5′-phosphatase (SHIP) in phagocytosis mediated by Fc gamma receptors and complement receptor 3 (alpha(M)beta(2); CD11b/CD18). J Exp Med 2001;193:61–71. [PubMed: 11136821]
47. Ai J, Maturu A, Johnson W, Wang Y, Marsh CB, Tridandapani S. The inositol phosphatase SHIP-2 down-regulates FcgammaR-mediated phagocytosis in murine macrophages independently of SHIP-1. Blood 2006;107:813–820. [PubMed: 16179375]
48. Whitman M, Downes CP, Keeler M, Keller T, Cantley L. Type I phosphatidylinositol kinase makes a novel inositol phospholipid, phosphatidylinositol-3-phosphate. Nature 1988;332:644–646. [PubMed: 2833705]
49. Gallois A, Klein JR, Allen LA, Jones BD, Nauseef WM. Salmonella pathogenicity island 2-encoded type III secretion system mediates exclusion of NADPH oxidase assembly from the phagosomal membrane. J Immunol 2001;166:5741–5748. [PubMed: 11313417]
50. Simonsen A, Lippe R, Christoforidis S, Gaullier JM, Brech A, Callaghan J, Toh BH, Murphy C, Zerial M, Stenmark H. EEA1 links PI(3)K function to Rab5 regulation of endosome fusion. Nature 1998;394:494–498. [PubMed: 9697774]
51. Shin HW, Hayashi M, Christoforidis S, Lacas-Gervais S, Hoepfner S, Wenk MR, Modregger J, Uttenweiler-Joseph S, Wilm M, Nystuen A, Frankel WN, Solimena M, De Camilli P, Zerial M. An enzymatic cascade of Rab5 effectors regulates phosphoinositide turnover in the endocytic pathway. J Cell Biol 2005;170:607–618. [PubMed: 16103228]

52. Chavrier P, Parton RG, Hauri HP, Simons K, Zerial M. Localization of low molecular weight GTP binding proteins to exocytic and endocytic compartments. Cell 1990;62:317–329. [PubMed: 2115402]

53. Karlsson K, Carlsson SR. Sorting of lysosomal membrane glycoproteins lamp-1 and lamp-2 into vesicles distinct from mannose 6-phosphate receptor/gamma-adaptin vesicles at the trans-Golgi network. J Biol Chem 1998;273:18966–18973. [PubMed: 9668075]

54. Nishio M, Watanabe K, Sasaki J, Taya C, Takasuga S, Iizuka R, Balla T, Yamazaki M, Watanabe H, Itoh R, Kuroda S, Horie Y, Forster I, Mak TW, Yonekawa H, Penninger JM, Kanaho Y, Suzuki A, Sasaki T. Control of cell polarity and motility by the PtdIns(3,4,5)P3 phosphatase SHIP1. Nat Cell Biol 2007;9:36–44. [PubMed: 17173042]

55. Ellson CD, Gobert-Gosse S, Anderson KE, Davidson K, Erdjument-Bromage H, Tempst P, Thuring JW, Cooper MA, Lim ZY, Holmes AB, Gaffney PR, Coadwell J, Chilvers ER, Hawkins PT, Stephens LR. PtdIns(3)P regulates the neutrophil oxidase complex by binding to the PX domain of p40(phox). Nat Cell Biol 2001;3:679–682. [PubMed: 11433301]

56. Allen LA, Allgood JA, Han X, Wittine LM. Phosphoinositide3-kinase regulates actin polymerization during delayed phagocytosis of Helicobacter pylori. Journal of leukocyte biology 2005;78:220–230. [PubMed: 15809290]

57. Pitt A, Mayorga LS, Stahl PD, Schwartz AL. Alterations in the protein composition of maturing phagosomes. The Journal of clinical investigation 1992;90:1978–1983. [PubMed: 1430221]

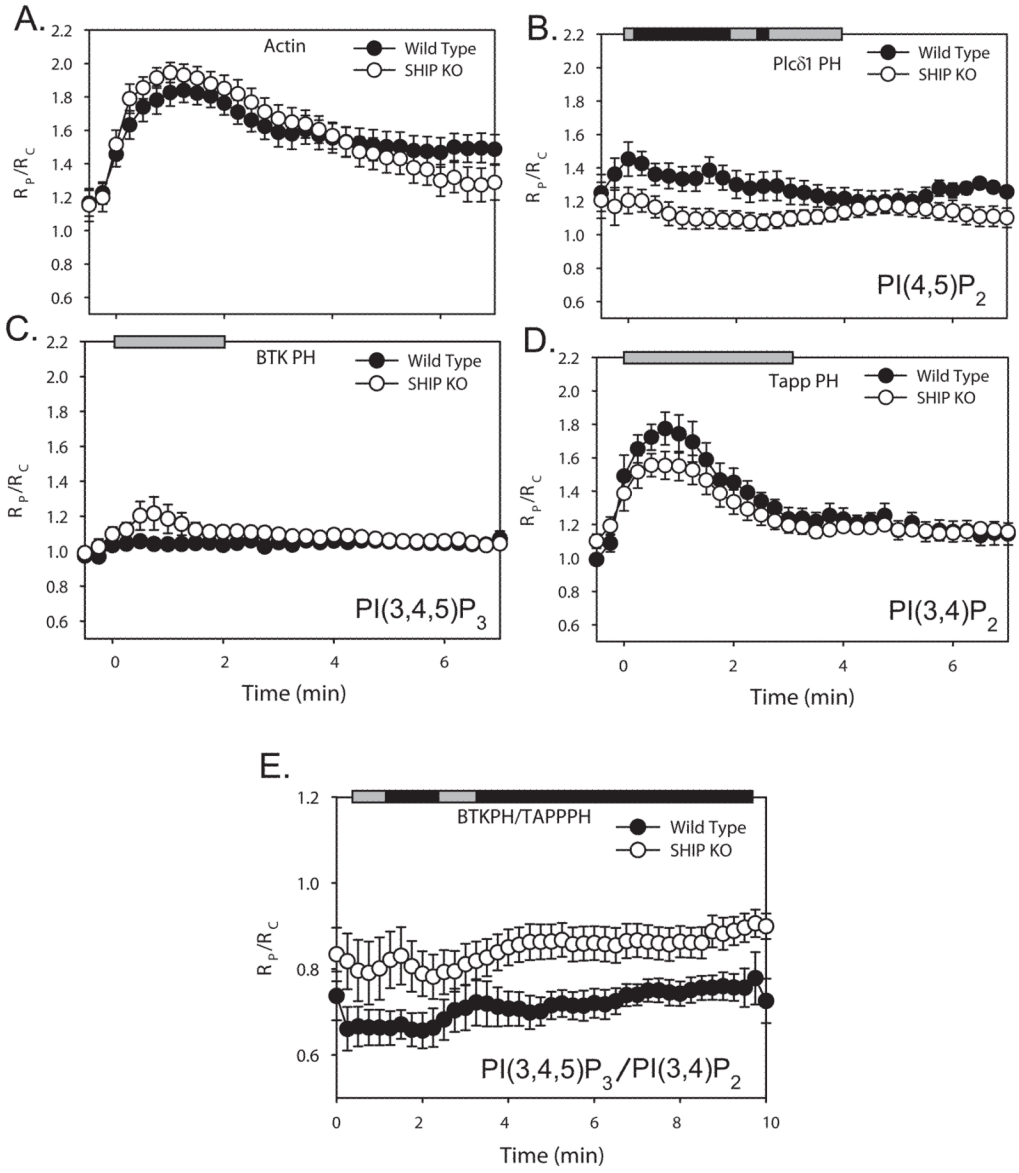

Figure 1.

Localization dynamics of actin-YFP and fluorescent PH domains tracking phosphoinositides. (A–D) R_P/R_C measured the localization of YFP chimeras to phagosomes, relative to free CFP, averaged over multiple events, in wild-type (black circles), and SHIP1$^{-/-}$ macrophages (white circles). Phagocytosis was completed in 3–5 mins. Error bars represent standard error of the mean (SEM). Horizontal bars indicate Student's t-test for significant differences. Grey bars indicate p-value > 0.05; black bars indicate data with p-value < 0.05. (A) Actin-YFP on the phagosome during phagocytosis (WT n=17, KO n=24). (B) Plcδ1PH-CIT recruitment (WT n=10, KO n=10). (C) BtkPH-CIT recruitment (WT n=10, KO n=8). (D) Tapp1PH-CIT recruitment (WT n=12, KO n=10). (E) BtkPH-CIT and TappPH-CFP on the phagosome during phagocytosis. (WT n=10, KO n=9). The ratio between BtkPH-CIT and TappPH-CFP was measured and plotted as R_P/R_C.

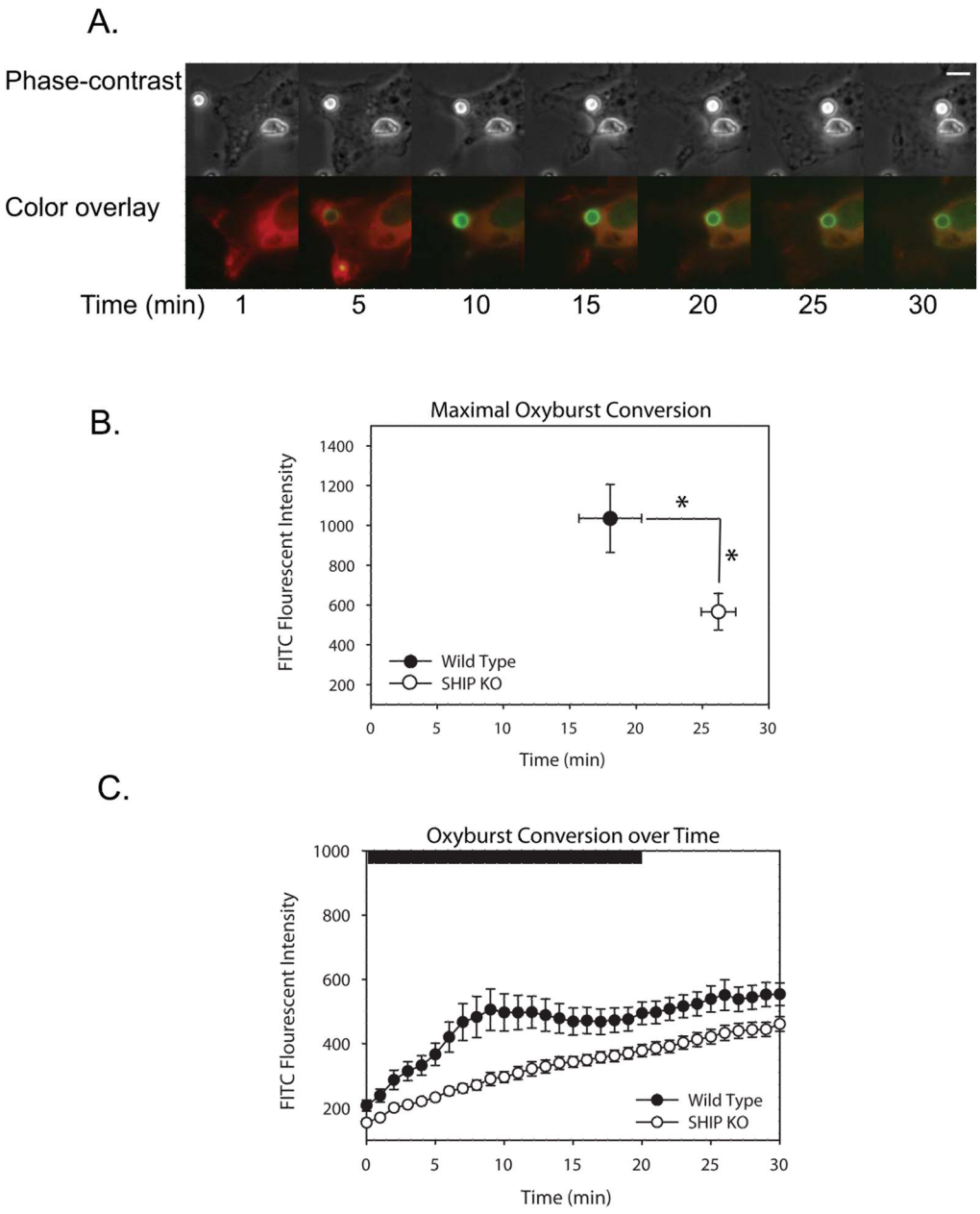

Figure 2.

Characterization of the early oxidative burst in wild-type or SHIP1$^{-/-}$ macrophages. Oxyburst-conjugated, IgG-opsonized beads were fed to wild-type or SHIP1$^{-/-}$ macrophages expressing β actin-mCherry and the increases in oxyburst fluorescence were recorded at regular intervals. (A) Phase-contrast and Overlay images of a wild-type macrophage undergoing phagocytosis of particles. Actin is pseudocolored red, oxyburst is pseudocolored green. Scale bar in the Phase-contrast image corresponds to 5 μm. (B) The maximal oxyburst fluorescence produced on the beads was plotted vs. the time of peak fluorescence for wild-type (n=20) or SHIP1$^{-/-}$ (n=27) macrophages. Asterisks indicate significance (p-value < 0.05) for both the difference in peak fluorescence intensity and time of peak fluorescence. (C) The level of oxidase activity, as indicated by the rise in fluorescence intensity, was averaged over time in multiple phagosomes from wild-type (n=15) or

SHIP1$^{-/-}$ (n=25) macrophages and plotted. Bar indicates Student's t-test for significant differences. Black bar corresponds to time points with significantly different fluorescence (p-value < 0.05).

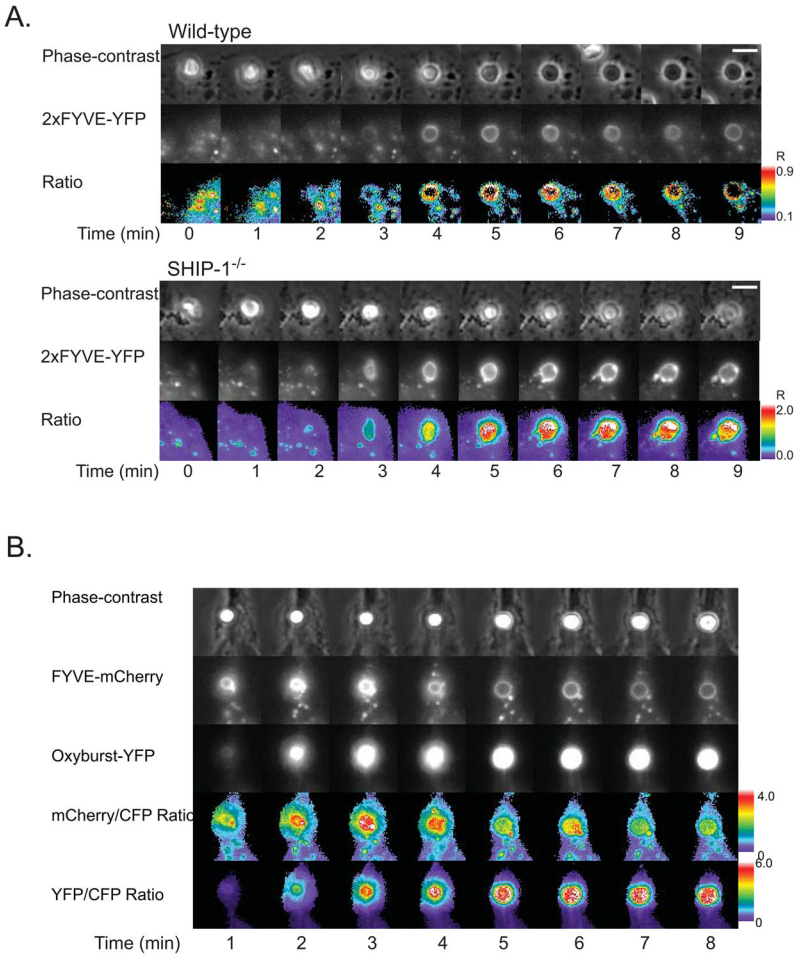

Figure 3.

Phase-contrast and ratiometric fluorescence microscopy of PI(3)P and the oxidative burst during phagocytosis of IgG-opsonized erythrocytes or oxyburst-coated particles. (A, B) Dynamics of 2xFYVE-YFP in wild-type (A) and SHIP−/− (B) macrophages. Phase-contrast (top), YFP (middle) and Ratio (bottom) image time-series of BMDM from either wild-type or SHIP1$^{-/-}$ mice during FcR-mediated phagocytosis. Scale bars in the Phase-contrast images equal 5 μm. Color bars indicate the range of the calculated R_M in the Ratio time series. 2xFYVE-YFP localized to the phagosome after initiation of phagocytosis in both wild-type and SHIP1$^{-/-}$ macrophages, but persisted on the phagosome in the absence of SHIP-1. (B) Relative dynamics of PI(3)P and the oxidative burst during phagocytosis in wild-type macrophages. Oxyburst-conjugated, IgG-opsonized beads were fed to macrophages expressing 2xFYVE-mCherry and CFP. Phase-contrast, mCherry, YFP, and Ratio of mCherry/CFP and YFP/CFP images showing time series of BMDM phagocytosing an oxyburst-coated bead. Colored bar indicates scale of ratio.

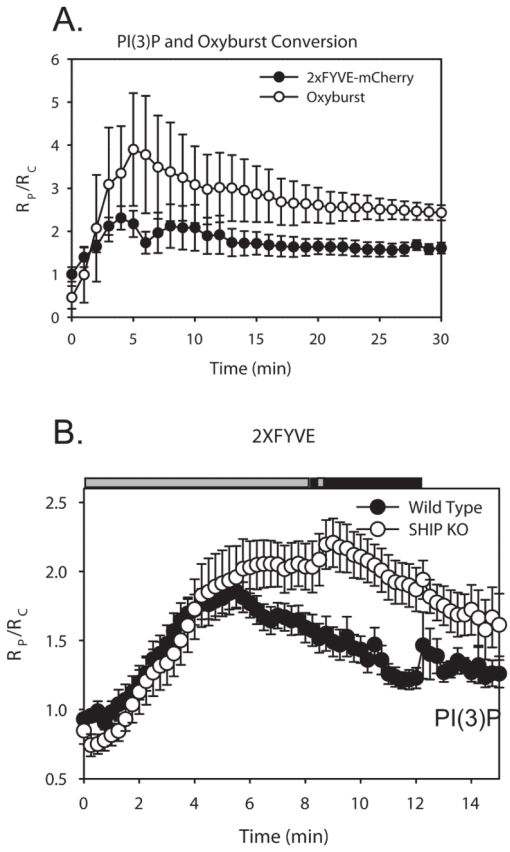

Figure 4.

Dynamics of PI(3)P and oxyburst conversion during phagocytosis in macrophages. (A) Plot of R_P/R_C depicting the increase in PI(3)P levels (FYVE-mCherry) and oxidase activation (Oxyburst) vs. time during phagocytosis (n=5). Error bars represent SEM. (B) PI(3)P dynamics in wild-type (black circles, n=13) and SHIP1$^{-/-}$ (white circles, n=9) macrophages expressing 2xFYVE-CIT and CFP. Plot of R_P/R_C indicates the dynamics of 2xFYVE-CIT during phagocytosis of IgG-opsonized erythrocytes. Horizontal bars indicate Student's t-test for significant differences. Grey bars indicate p-value > 0.05, black bars indicate data with p-value < 0.05.

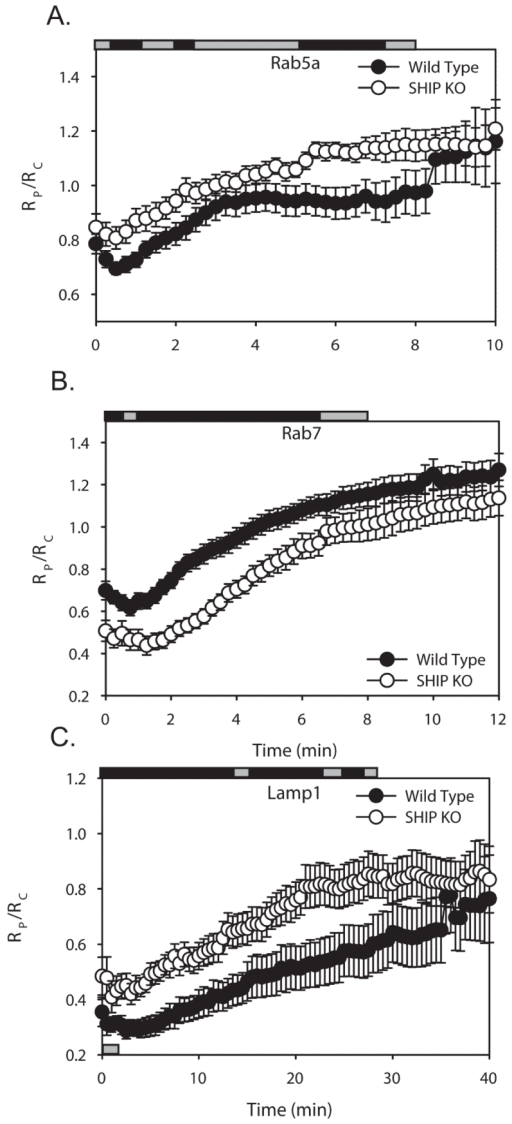

Figure 5.

Localization dynamics of endocytic markers during phagocytosis of IgG-opsonized erythrocytes in wild-type (black circles) or SHIP1$^{-/-}$ (white circles) macrophages. (A) Tracking indicated the rise of the early endosome probe Rab5a-CIT on the phagosome after initiation of phagocytosis in wild-type (n=14) or SHIP1$^{-/-}$ (n=16) macrophages. (B) Tracking indicated the rise of the late endosome probe Rab7-YFP on the phagosome membrane after its initial exclusion from the forming phagosome in wild-type (n=18) or SHIP1$^{-/-}$ (n=14) macrophages. (B) Tracking showed the recruitment of the lysosomal marker Lamp1-YFP on phagosomes during phagosome maturation in wild-type (n=16) or SHIP1$^{-/-}$ macrophages (n=18). Error bars represent SEM. Horizontal bars indicate Student's t-test for significant differences. Grey bars indicate insignificant differences, black bars indicate data with p-values < 0.05.

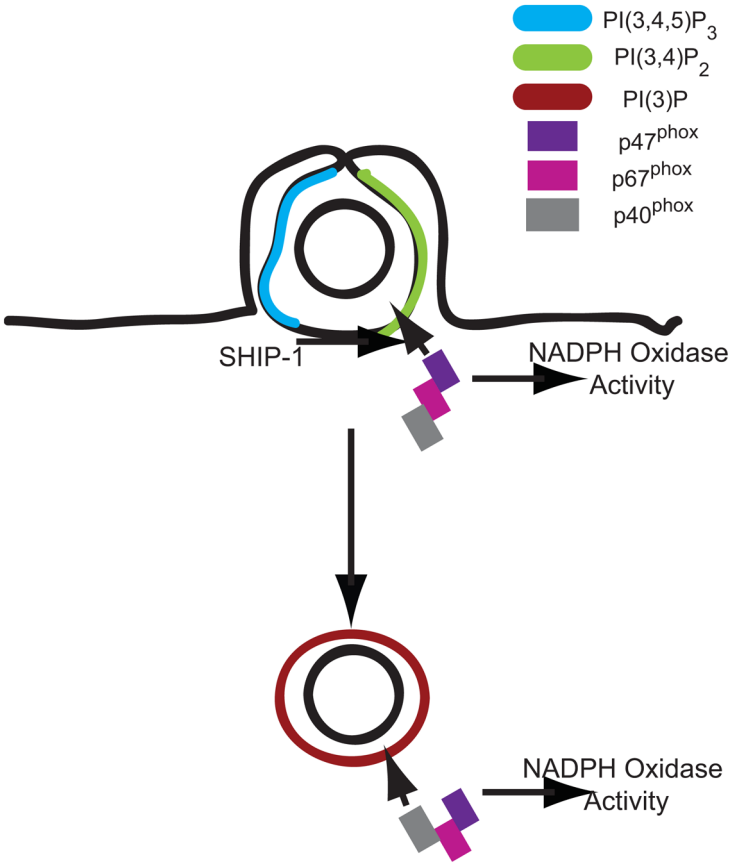

Figure 6.